Vacuum infusion as a novel method to determine wood permeability

Andrey Pereira Acosta (andrey.acosta@ufrgs.br)
Federal University of Rio Grande do Sul https://orcid.org/0000-0002-5074-3772
Kelvin Techera Barbosa
Federal University of Pelotas: Universidade Federal de Pelotas
Amanda Albertin Xavier da Silva
Federal University of Rio Grande do Sul: Universidade Federal do Rio Grande do Sul
Darci Alberto Gatto
Federal University of Pelotas: Universidade Federal de Pelotas
Rafael de Avila Delucis
Federal University of Pelotas: Universidade Federal de Pelotas
Sandro Campos Amico
Federal University of Rio Grande do Sul: Universidade Federal do Rio Grande do Sul

Research Article

Keywords: Capillary pressure, wood morphology, vacuum infusion, porous material

Posted Date: August 11th, 2022

DOI: https://doi.org/10.21203/rs.3.rs-1689188/v1

Abstract

This study aims to propose a novel method, vacuum infusion process, to measure the longitudinal permeability of wood. The vacuum infusion method uses a vacuum bag sealed over the fibrous material, with a vacuum inlet and a vacuum outlet. It can be performed on top of any flat surface, and its process is relatively swift. Six different woods (*Pinus elliottii*, *Araucaria angustifolia*, *Ochroma pyramidale*, *Cedrela fissilis*, *Tectona grandis*, and *Eucalyptus grandis*) and three different fluids (water, soybean oil, and furfuryl alcohol) were selected for the study. After preliminary evaluations of morphology, chemical characteristics, density, porosity, contact angle and capillary pressure, three woods and two fluids were selected for the actual permeability measurements. The highest permeability was obtained for the *Ochroma pyramidale* wood, being $0.45–7.49\times10^{-11}$ m^2. This wood was 58–88% and 18–62% more permeable than the *Pinus elliottii* and *Eucalyptus grandis* woods, respectively. The fluid was found to have some influence on the experiment and therefore must be carefully selected. The difference in permeability of the woods was attributed to morphological characteristics, especially the presence of axial vessels, which are 60% larger for *Ochroma pyramidale* wood compared to *Eucalyptus grandis* wood, while *Pinus elliottii* has no vessels. The amount of voids in all woods, nevertheless, was similar, as well as the evaluated chemical characteristics and structural anatomical elements (tracheids and/or fibers). In all, the determination of apparent permeability using the vacuum infusion process is practical and with good accuracy, yielding results similar to those from other methods in the literature.

1. Introduction

Wood permeability plays an important role in impregnation rate and retention of the impregnated substances, as well as the consequent changes in other properties (Tarmian et al. 2020). Wood permeability depends on some of its physical and chemical characteristics and may vary according to both genus and species. The wood permeability depends on some of its physical and chemical characteristics and may vary according to both genus and species. From a morphological point of view, the vessels (in hardwoods) and tracheids (in softwoods) have a direct influence on wood permeability. Furthermore, regarding chemical features, the content and composition of extractive compounds may be considered as main factors, that affect wood permeability.

The wood vessels are the main liquid conducting tissues in hardwoods. These anatomical elements are responsible for 90% of the transported water and their content may vary from 10 to 60% in relation to the total area in the transverse plane (Bajpai 2018). Furthermore, diameter, clustering form, and perforation type of these vascular elements also affect wood permeability (Mahdian et al. 2020). (Rezende et al. 2018) evaluated the water permeability of two eucalypt woods and observed that the wood with the smallest vessel diameter (*Eucalyptus dunnii* wood) showed a permeability mean 10% smaller than the same property of the wood with the largest vessel diameter (*Eucalyptus grandis* wood). (Rogério et al. 2010) compared the water permeability of other two eucalypt woods (*Eucalyptus grandis* and *Corymbia citriodora*) and concluded that the permeability of the *Eucalyptus grandis* wood was about 20% higher due to the average diameter of its vessels, which was 50% larger. (Emaminasab et al. 2015) affirmed that

the effectiveness of the vessels in conducting liquids is due to their large diameter and the presence of perforations that axially connect them to each other.

Regarding softwoods, the tracheids are the main fluid conducting anatomical elements and correspond to about 90% of the overall morphological constitution in volume (Brändström 2001). The smaller diameter of the tracheids from softwoods in relation to vessels from hardwoods explains the lower permeability of softwoods compared to hardwoods (Emaminasab et al. 2015). Thus, tracheids differ from vascular and other axial anatomical elements due to their small diameters and absent perforations (i.e. they are not axially interconnected) (Emaminasab et al. 2015). Although they have no axial perforations, the tracheids are laterally interconnected by small openings called radial pits, which vary in diameter from 0.2 to 20 µm (Zabel and Morrell 2020). In this regard, (Lehringer et al. 2009) stated that the presence of obstructed pits, usually caused by internal pressure differences during wood drying processes is a limiting factor for permeability in softwoods. This obstruction process, known as tylosis, is irreversible since involves the formation of hydrogen bonds between the torus/margo and the pit opening.

Several methods have been developed for measuring wood permeability (Ahmed and Chun 2009; Bufalino et al. 2013; Taghiyari et al. 2014; Ai et al. 2017b; Rezende et al. 2018). (Ai et al. 2017a), for example, developed a complex and costly system that consisted of two identical rigid stainless-steel tanks connected in series to a sample holder, a vacuum valve, actuators and pressure gauges attached at each end. The pressure vessels were also connected to a vacuum pump at one end and to the fluid reservoir at the other one. The fluid passed through the wood, and the permeability was measured based on the pressure difference between inlet and outlet.

(Ahmed and Chun 2009) proposed a simple process for measuring wood permeability. The authors inserted a small prismatic *Samanea saman* wood sample into a Petri dish and poured a dye solution (10 g of safranin diluted in 500 mL of 50% ethyl alcohol solution). The infiltration speed of the safranin solution was measured using a microscope aided by a software for image processing. This method was found unreliable due to the difficulty in monitoring the flow front justified by the heterogeneous flow inside the wood.

More recently, (Leggate et al. 2019) measured the longitudinal permeability of *Pinus elliottii* and *Pinus caribaea* woods. The samples were sealed on their lateral surfaces with epoxy resin and then impregnated with water at a constant pressure of 4.20 MPa. Wood permeability was measured using a Porolux 1000 equipment (commonly used industrially), which consists of a sample holder placed on an analytical scale, which is connected to a pressure vessel and a manometer monitored by a computer. This method, however, has a high cost associated with the device, and the benchtop equipment could not be easily moved, restricting its use.

Nonetheless, the most efficient method published before was developed by (Taghiyari et al. 2014). In this equipment, two milli-second precision electronic clocks allow a high accuracy fluid movement capture. This apparatus consists in a changeable glass-made cylinder column with a variable length (from 30 cm

to 2 m) (Esmailpour et al. 2019). In all, the permeability tests already designed for analyzing wood parts are limited by the required sample shapes and the low measurement accuracy.

The vacuum infusion process, commonly used as a manufacturing method for polymeric composites, is proposed in this work as a novel way to measure wood permeability. In this process, the sample is placed on a smooth and rigid surface and then sealed with the aid of a polymeric film and a sealing tape (Alms et al. 2010). Channels for vacuum application and fluid injection are positioned and a vacuum pump is used to evacuate the air from the mold and sample. The vacuum drives the impregnation of the porous material, simultaneously flowing in the plane and through the thickness due to the pressure gradient applied between inlet and outlet ends (Summerscales and Searle 2005). A camera can be used to monitor the resin flow, allowing calculation of the permeability based on Darcy's law.

The infusion process has high versatility, the shape of the sample can vary, the material cost is low, the system is simple and easily transported, and requires an easy operation, being commonplace in the composites industry. The vacuum infusion process is relatively recent (around two decades ago), but has been successfully used for measuring permeability of fibrous mats and fabrics, which are used as reinforcements in composites (Li et al. 2015; Aitomäki et al. 2016; Yun et al. 2017; da Silva et al. 2020). For instance, (da Silva et al. 2020) determined the in-plane permeability of R-glass and aramid-based fabrics positioned in different stacking sequences by vacuum infusion. They adjusted a constant pressure of -100 kPa between inlet and outlet ends and the reported values ranging from 2.95×10^{-11} to 8.27×10^{-11} m^2. In this context, this work introduces a novel method, vacuum infusion, to measure the longitudinal wood permeability.

2. Materials And Methods

2.1 Raw material

1 mm thick wood veneers cut by rotary peeling from six wood species, namely *Pinus elliottii*, *Araucaria angustifolia*, *Ochroma pyramidale*, *Cedrela fissilis*, *Tectona grandis*, and *Eucalyptus grandis*, were acquired from different Brazilian companies, Ecofolhas (Pinheiros/SP), ArtBalsa (Florianopolis/SC) and Léo Madeiras (Curitiba/PR). These species were chosen due to both the great differences in anatomical features and commercial availability between each other.

Three impregnating fluids were used in the experiments:

(i) deionized water, a polar liquid commonly used for measuring permeability in woods, with a density of 1.005 g/cm³ and dynamic viscosity of 1.05 cP;
(ii) soybean oil (purchased from Klemm (Santa Cruz do Sul/Brazil)), an inexpensive, non-toxic, and non-polar liquid, with a density of 0.899 g/cm³ and dynamic viscosity of 74.92 cP;
(iii) furfuryl alcohol (purchased from Sigma Aldrich (São Paulo/Brazil)), a resin commonly used to impregnate solid woods, with a density of 1.136 g/cm³ and dynamic viscosity of 5.0 cP.

Specific gravity was considered as the simple ratio between the mass and volume for each fluid. And the dynamic viscosity was determined using a Brookfield viscometer (#3 spindle) at room temperature (~ 25 ºC).

2.2 Preliminary characterization

Oven-dried (at 103°C for 24 h) wood fragments cut from the veneers were prepared (Tappi T257 2012) and characterized via wet chemical analyses to obtain moisture (Tappi 2007), ashes (Tappi T 211 om-02 2002), ethanol–toluene extractives (TAPPI T 204 cm-97 2012), acid-insoluble lignin (Tappi T222 Om-02 2011), and holocellulose (remaining mass up to 100%) contents. Sections of the woods were prepared with 13 µm-thick on a Microtome (MRP2015), were dyed with an alcoholic solution of malachite green and then morphologically analysed using an optical microscope adjusted to a magnification of 25 times and a free software called ImageJ. Apparent density (ρ_a), basic density (ρ_b), moisture content (MC), and porosity (Ø) were evaluated. The latter is shown in Eq. 1 described by (Siau 1984). A digital caliper (resolution of 0.01 mm) and an analytical scale (resolution of 0.001 g) were used to determine dimensions and mass, respectively.

$$Ø = 1 - \rho b\,[(0.685 + 0.01 \cdot MC)/\rho a] \quad (1)$$

Tangential surface hydrophobicity was evaluated by measuring the static contact angle at six different times from 5 s to 120 s after the contact of a 50 µl droplet of each liquid using a DSA25 equipment (Kruss® brand) according to the sessile drop method. Capillary pressure (P_c) was determined based on the methodology described in (Amico and Lekakou 2002). For that, a metal rod supported a wooden veneer with the dimensions of 250 × 50 × 1 mm^3, which was immersed in the liquid to a depth of 10 mm (Fig. 1).

The test was ended when the liquid flow stabilized, in height and weight (around 72 h), followed using a ruler and an analytical scale (resolution of 0.01 g). After equilibrium, the capillary pressure (P_c, in Pa) is calculated according to Eq. 2.

$$P_c = \rho_f \times g \times h_e \quad (2)$$

where: ρ_f is fluid density ($g.cm^{-3}$), g is gravitational acceleration ($m.s^{-2}$), and h_e is the equilibrium height (m).

2.3 Apparent permeability evaluation

Three different woods (*Pinus elliottii*, *Ochroma pyramidale*, and *Eucalyptus grandis*) were selected based on their dissimilarity in terms of the previous physical and chemical results. Moreover, the permeability tests for soybean oil and furfuryl alcohol were successfully carried out at a -1.0 MPa vacuum, which yielded a too fast liquid movement when the water was selected as infiltrating liquid. This impaired the permeability measurement in this case and can be attributed to the small viscosity and high polarity of

the deionized water. Because of that, the permeability experiment was later performed at -0.5 MPa for the water.

The permeability experiment was performed at room temperature (~ 25°C), in duplicate for each wood/liquid combination. For that, two 120 mm-long plastic spiroducts were connected to the inlet and outlet hoses, forming a rectangular injection area of 120 × 300 mm^2 on a smooth surface. At one end, the inlet hose was connected to a 2 L beaker, in which the fluid was previously poured. At the other end, the outlet hose was attached to a pressure pot, connected to a vacuum pump.

A rectangular wooden veneer with dimensions of 120 × 300 × 1 mm^3 was placed between spiroducts and a vacuum bag was placed on top to seal the injection area with the aid of a tacky-tape. After that, the vacuum pump was adjusted to a constant pressure of -92 kPa yielding a predominantly unidirectional flow front, which was monitored using a digital camera. Transverse marks, 30 mm apart, were made on the wood veneer to allow easy flow-front observation. Figure 2 illustrates the vacuum infusion system. Some of the consumables, i.e., hoses, spiroducts, connections and valves, were reused, minimizing disposal and the associated environmental impact.

The ImageJ software was used to obtain the flowfront position from the acquired photographs (a minimum of 20 for each experiment). After collecting the data, a graph of squared flow front position × time was plotted and linear regression was applied, considering a minimum r^2 of 0.95. From the slope of this line, it was possible to calculate apparent in-plane permeability (κ, in m^2) based on Eq. 3, reported in Rudd et al. (1997). This equation for rectilinear flow under constant pressure is based on Darcy's Law, which states that the flow velocity is proportional to the pressure gradient (Caglar et al. 2018).

$$\kappa = \frac{(\emptyset \cdot \mu)}{(2 \cdot P_o) \cdot (X^2_{ff}/t)} \qquad (3)$$

where: £ is preform porosity, μ is fluid viscosity (cP), P_o is injection pressure (92 kPa), X^2_{ff} is the flow front position (m), and t is the infiltration time (s).

All data, except the chemical analyses, capillary pressure and contact angle results, were subjected to ANOVA analysis of variance. Homogeneity of variances and data normality were verified using Shapiro-Wilk tests. Whenever the null hypothesis was rejected, General Linear Model (GLM) tests were used to compare the means. All statistical analyses were implemented at a significance level of 5%.

3. Results And Discussion

Figure 3 shows the chemical characteristics of the studied woods. The highest holocellulose content was observed for *Eucalyptus grandis* wood (69.51%), followed by *Cedrela fissilis* wood (69.02%) and *Ochroma pyramidale* wood (69.02%). The highest lignin content was observed for *Tectona grandis* wood (38.11%),

followed by *Araucaria angustifolia* wood (34.90%) and *Pinus elliottiii* wood (30.27%). High extractives contents were found for *Ochroma pyramidale* wood (6.35%), *Tectona grandis* wood (5.25%) and *Cedrela fissilis* wood (4.90%). These results can be attributed to the wood natures since the hardwoods presented higher holocellulose and extractives contents, while the softwoods presented higher lignin contents, except for the *Tectona grandis* wood. These results are similar to those reported in the literature, i.e., 60–70% range for holocellulose content, 20.5–38.5% range for lignin content, and 1–10% range for extractives content (Severiano et al. 2010; Esteves et al. 2013; Borrega et al. 2015; Lengowski et al. 2020; Acosta et al. 2021b).

Figure 4 shows cross-sectional images of the studied woods. The *Pinus elliottii* wood shows some resin canals, which are elongated, tube-shaped intercellular spaces surrounded by epithelial cells.

The optical micrographs also confirmed the large differences in terms of diameter of the main liquid conducting anatomical elements from softwoods (c.a. tracheids) and hardwoods (c.a. vessels), i.e., the latter were 10–20 times wider. Table 1 shows anatomical characteristics acquired from the aforementioned optical micrographs. Among the studied softwoods, *Araucaria angustifolia* showed the largest tracheid diameter ($Ø_F$) and lumen diameter ($Ø_{FL}$). And the *Cedrela fissilis* wood was the hardwood with the widest vessels ($Ø_V$), in a decreasing order, followed by *Ochroma pyramidale*, *Eucalyptus grandis* and *Tectona grandis*. Regarding the radial ray width, the *Ochroma pyramidale* wood stood out compared to the other woods. These ducts are not found in hardwoods. The presence of vessels in the hardwoods shown here is an important anatomical difference between hardwoods and softwoods. Softwoods have a simpler morphological structure, which can be explained by the biological evolution of these plants, being botanically classified as primitive vegetables.

Table 1
– Anatomical properties of the woods.

Wood specie	$Ø_F$ (µm)	$Ø_V$ (µm)	$Ø_{LF}$ (µm)	$Ø_{LV}$ (µm)	R (µm)	L_F (mm)
Pinus elliottii	25.88 (5.6) c	-	22.01 (2.80) d	-	21.67 (5.93) c	2.39 (0.51) d
Araucaria angustifolia	46.86 (4.6) d	-	41.57 (8.01) e	-	18.46 (4.03) b	2.67 (0.69) e
Cedrela fissilis	7.77 (1.5) b	482.78 (13.1) c	6.01 (0.30) c	446.13 (53.38) c	12.89 (4.27) a	0.79 (0.27) ab
Ochroma pyramidale	4.88 (0.59) a	372.30 (40.3) b	4.12 (0.80) b	367.83 (52.38) b	95.76 (12.12) e	1.29 (0.23) c
Tectona grandis	3.20 (0.85) a	214.24 (10.18) a	2.68 (0.48) a	200.73 (61.57) a	89.04 (17.15) d	0.59 (0.08) a
Eucalyptus grandis	4.70 (1.15) a	223.72 (51.6) a	4.12 (0.80) b	201.88 (43.31) a	21.69 (5.93) c	0.94 (0.23) b

where: $Ø_F$ is fiber diameter, $Ø_V$ is vessel diameter, $Ø_{LF}$ is fiber lumen diameter, $Ø_{LV}$ is vessel lumen diameter, R is ray width, L_F is fiber length (note: different letters represent significant differences in the column).

Table 2 shows the apparent density, basic density, moisture content and porosity results for the studied woods. The *Tectona grandis* wood showed the highest apparent and basic densities, justified by the small diameter of its anatomical elements, especially vessels and fiber lumens, and the consequent high lignin content since it is mostly likely located in the middle lamella between fibers. The *Ochroma pyramidale* wood presented the smallest density, which is attributed to its wide fibers and vessels, as well as its high porosity. The values found in this study are in agreement with those reported in the literature for all woods, 0.15–0.60 g/cm^3 for apparent density and 0.11–0.55 g/cm^3 for basic density (Valério Alvaro, Watzlawick et al. 2008; Zanella et al. 2016; Mahdian et al. 2020; Acosta et al. 2021a).

Table 2
– Physical properties of the woods.

Wood specie	ρ_a (g/cm³)	ρ_b (g/cm³)	MC (%)	Ø (%)
Pinus elliottii	0.59 (0.050) cd	0.49 (0.041) d	9.97 (1.99) ab	46.55 (2.25) a
Araucaria angustifolia	0.54 (0.015) c	0.47 (0.008) cd	10.67 (1.16) ab	49.85 (1.98) b
Cedrela fissilis	0.48 (0.083) b	0.44 (0.073) c	11.16 (0.30) ab	58.31 (1.81) c
Ochroma pyramidale	0.18 (0.022) a	0.15 (0.017) a	9.18 (2.41) a	73.88 (1.49) d
Tectona grandis	0.61 (0.027) d	0.54 (0.062) e	11.35 (0.90) b	44.96 (1.59) a
Eucalyptus grandis	0.45 (0.017) b	0.39 (0.018) b	10.62 (0.53) ab	56.47 (2.11) c

where: ρ_a is apparent density, ρ_b is basic density, MC is moisture content, £ is porosity (note: different letters above the bars represent significant differences).

Among the studied woods, *Tectona grandis* and *Eucalyptus grandis* woods presented the largest water contact angles (Fig. 5a). These two woods were followed by *Cedrela fissilis* wood, *Araucaria angustifolia* wood, *Pinus elliottii* wood, and *Ochroma pyramidale* wood in a decreasing order of water contact angle. These contact angles can be ascribed to the fiber length of the woods since the smaller was the fiber length, the higher was the contact angle. On the other hand, all woods presented more similar contact angles results when soybean oil or furfuryl alcohol were used (Figs. 5b-5c), with a slightly higher value again for *Tectona grandis* and *Eucalyptus grandis* with soybean oil. In all cases, the contact angles for all liquids decreased up to 10–15 s, mostly stabilizing after that. Previous studies reported significant correlations of contact angle values and chemical (Kishino and Nakano 2004; Rossi et al. 2012), anatomical (Piao et al. 2010) (Oberhofnerová and Pánek 2016), and other physical properties (Amorim et al. 2013), which did not occur in the present study.

Figure 6 shows the height of the flow front in the capillary experiments for the studied woods. The values progressively increased until about 72 h, with little change after that until 160 h. These same three woods stood out in terms of both the soybean oil and furfuryl alcohol capillary pressures. In the case of the softwoods, these results can be ascribed to their high tracheid length and tracheid diameter. (Ahmed and Chun 2011) stated that the capillary pressure of a softwood is inversely proportional to its tracheid lumen diameter, which corroborates the findings of the current work.

On the other hand, the *Ochroma pyramidale* wood presented high capillary pressure probably due to its high porosity, which indicates that this physical property is a better permeability indicator than vessel diameter or length. In hardwoods, the porosity is dependent on both anatomical properties and presence of some anatomical elements, especially vessels, which explains the obtained result.

For water as the infiltrating fluid, the *Pinus elliottii* wood presented the highest value (Table 3), followed by *Ochroma pyramidale* wood and *Araucaria angustifolia* wood. For soybean oil as the infiltrating fluid, the *Ochroma pyramidale* wood presented the highest value, followed by *Pinus elliottii* wood and *Araucaria angustifolia* wood. For furfuryl alcohol as the infiltrating fluid, the *Pinus elliottii* wood presented the highest value, followed by *Ochroma pyramidale* wood and *Araucaria angustifolia* wood.

Table 3
– Capillary pressure of woods.

	Water		**Soybean oil**		**FA**	
Wood specie	**Sample I**	**Sample II**	**Sample I**	**Sample II**	**Sample I**	**Sample II**
Pinus elliottii	1716.75	1618.65	1499.26	1583.04	1829.07	1839.09
Araucaria angustifolia	1177.20	1137.96	1146.49	1631.55	2061.86	1696.05
Cedrela fissilis	588.60	539.55	749.63	811.36	1030.93	1053.10
Ochroma pyramidale	1422.45	1451.88	1631.55	1675.64	1884.50	1828.07
Tectona grandis	735.75	686.70	617.34	705.53	587.52	609.69
Eucalyptus grandis	441.45	490.50	811.36	793.72	1053.10	1030.93

The capillary pressure results did not show a direct correlation with the previous contact angles results, which suggests that it is probably affected by bulk anatomical and chemical characteristics and not only surface ones.

Due to their differences (anatomical and chemical), only three wood species were selected for permeability studies. The *Ochroma pyramidale* wood was chosen due to its large vessel diameter and high porosity, and *Eucalyptus grandis* due to its large availability in Brazil. Among the softwoods, *Pinus elliottii* was selected since *Araucaria angustifolia* is a native wood in Brazil and there are restrictive laws regarding its exploitation.

Figure 7 shows the flow front position (X_{ff}) and Fig. 8 shows the squared flow front position squared (X_{ff}^2) as a function of the injection time data for the selected woods. The *Ochroma pyramidale* wood showed the fastest flow front for both liquids, which can be partly explained by its significantly higher porosity compared to the other woods. Although the infiltration is affected by capillary pressure, this is a comparatively small driving force in the permeability experiment and indeed it did not show a direct correlation.

Compared to furfuryl alcohol, the soybean oil was approximately 5 times slower to permeate the wood, which is due to its higher viscosity (Zhang and Cai 2008). The lower chemical affinity with the wood, since these two compounds have a high degree of polarities, may also be partly responsible. Besides, the pattern of the flow front evolution for the soybean oil seems to be clearer than that of the furfuryl alcohol.

In that context, (Trindade et al. 2019) affirmed that, when the fluid flows more slowly, the determination of permeability is more accurate, depending on the balance between injection pressure and capillary pressure.

Figure 9 shows the calculated mean permeability values. Compared to the literature, the used methodology showed a smaller variability (maximum CV of 22.25%), which suggests that this method is more precise than those found in the literature (Table 4). The results obtained for the water were similar to those related to the other fluids, although they are not comparable since were measured at different pressure levels. This also indicates that other infiltrating fluids could be applied for measuring wood permeability by vacuum infusion.

Table 4
– Values of wood permeability reported in the literature.

Wood specie	Permeability range (× 10^{-11} m^2)	CV (%)	Infiltrating fluid	Reference
Pinus radiata	0.36–0.60	48–50	Water	(Booker 1990)
Eucalyptus grandis	1.2	55–57	Water	(Rezende et al. 2018)
Populus nigra	11–12	32	Water	(Emaminasab et al. 2015)
Pinus sp.	6–13	50	Water	(Leggate et al. 2021)
E. grandis e *E. citriodora*	5–6	25–28	Water and preservative	(Rogério et al. 2010)

The reported CV values ranged from 25–55%, depending on the selected wood specie, infiltrating fluid and measurement apparatus. The high variation in wood permeability has already been reported in the literature and could be attributed to the inhomogeneous wood morphology, including diameter, distribution and grouping of porous anatomical elements. Nevertheless, it may be seen that the values reported in the literature are in the same range of those found in the present study, considering the similarity between the viscosities of FA and water.

4. Conclusion

In this study, wood permeability was determined by a novel methodology based on vacuum infusion, which has been used to measure permeability of fibrous reinforcements used in polymer composites. Two fluids and three woods were selected for the permeability study after preliminary chemical, physical and anatomical analyses.

Contact angle and capillary pressure results did not directly correlate to each other, and neither with the wood permeability. Two of the three highest capillary pressures were obtained for softwoods, which

indicates a high influence of the tracheid diameter on this property.

Although the infiltration is affected by capillary pressure, this is a minor driving force in the permeability experiment carried out and indeed it did not show a direct effect on permeability. It was observed that the most porous woods were the most permeable ones, especially the *Ochroma pyramidale* wood.

In all, the vacuum infusion method proved to be a reliable process for measuring wood permeability. The values found for permeability agreed with the literature, however, the method used in the present study presented comparatively lower coefficient of variation than those reported. Thus, this methodology proves to be an accurate and practical alternative, able to be easily reproduced.

Declarations

ACKNOWLEDGEMENTS

This work was supported by Coordination for the Improvement of Higher Education - CAPES (code 001) and National Council for Scientific and Technological Development – CNPq (Financial code 301758/2019-0).

DISCLOSURE OF POTENTIAL CONFLICTS OF INTEREST

The authors declare that they have no known competing financial interests or personal relationships that could have appeared to influence the work reported in this paper.

References

1. Acosta A, Avila R De, Campos S, Alberto D (2021a) Fast-growing pine wood modified by a two-step treatment based on heating and *in situ* polymerization of polystyrene. Constr Build Mater 302:124422. https://doi.org/10.1016/j.conbuildmat.2021.124422
2. Acosta AP, Barbosa KT, Amico SC, et al (2021b) Improvement in mechanical, physical and biological properties of eucalyptus and pine woods by raw pine resin *in situ* polymerization. Ind Crops Prod 166:113495. https://doi.org/10.1016/j.indcrop.2021.113495
3. Ahmed SA, Chun SK (2009) Observation of liquid permeability related to anatomical characteristics in Samanea saman. Turkish J Agric For 33:155–163. https://doi.org/10.3906/tar-0807-13
4. Ahmed SA, Chun SK (2011) Permeability of T*ectona grandis* L. As affected by wood structure. Wood Sci Technol 45:487–500. https://doi.org/10.1007/s00226-010-0335-5
5. Ai W, Duval H, Pierre F, et al (2017a) A novel device to measure gaseous permeability over a wide range of pressures : characterisation of slip flow for Norway spruce , European beech , and wood-based materials To cite this version : HAL Id : hal-01523306
6. Ai W, Duval H, Pierre F, Perré P (2017b) A novel device to measure gaseous permeability over a wide range of pressures: Characterisation of slip flow for Norway spruce, European beech, and wood-

based materials. Holzforschung 71:147–162. https://doi.org/10.1515/hf-2015-0264

7. Aitomäki Y, Moreno-Rodriguez S, Lundström TS, Oksman K (2016) Vacuum infusion of cellulose nanofibre network composites: Influence of porosity on permeability and impregnation. Mater Des 95:204–211. https://doi.org/10.1016/j.matdes.2016.01.060
8. Alms JB, Garnier L, Glancey JL, Advani SG (2010) In-plane permeability characterization of the vacuum infusion processes with fiber relaxation. Int J Mater Form 3:1267–1275. https://doi.org/10.1007/s12289-010-0690-7
9. Amico SC, Lekakou C (2002) Axial impregnation of a fiber bundle. Part 1: Capillary experiments. Polym Compos 23:249–263. https://doi.org/10.1002/pc.10429
10. Amorim MRS, Ribeiro PG, Martins SA, et al (2013) Surface wettability and roughness of 11 amazonian tropical hardwoods. Floresta e Ambient 20:99–109. https://doi.org/10.4322/floram.2012.069
11. Bajpai P (2018) Wood and Fiber—Growth and Anatomy. Biermann's Handb Pulp Pap 75–103. https://doi.org/10.1016/b978-0-12-814240-0.00003-3
12. Booker RE (1990) Changes in transverse wood permeability during the drying of Dacrydium cupressinum and Pinus radiata. New Zeal J For Sci 20:231–244
13. Borrega M, Ahvenainen P, Serimaa R, Gibson L (2015) Composition and structure of balsa (*Ochroma pyramidale*) wood. Wood Sci Technol 49:403–420. https://doi.org/10.1007/s00226-015-0700-5
14. Brändström J (2001) Micro- and ultrastructural aspects of norway spruce tracheids: A review. IAWA J 22:333–353. https://doi.org/10.1163/22941932-90000381
15. Bufalino L, Mendes LM, Tonoli GHD, et al (2013) Relation of transverse air permeability with physical properties in different compositions of sugarcane bagasse particleboards. Mater Res 16:150–157. https://doi.org/10.1590/S1516-14392012005000164
16. Caglar B, Salvatori D, Sozer EM, Michaud V (2018) In-plane permeability distribution mapping of isotropic mats using flow front detection. Compos Part A Appl Sci Manuf 113:275–286. https://doi.org/10.1016/j.compositesa.2018.07.036
17. da Silva AAX, Souza JA, Manes A, Amico SC (2020) In-plane Permeability and Mechanical Properties of R-Glass/Aramid Hybrid Composites. J Mater Eng Perform 29:4484–4492. https://doi.org/10.1007/s11665-020-04944-1
18. Emaminasab M, Tarmian A, Pourtahmasi K (2015) Permeability of poplar normal wood and tension wood bioincised by *Physisporinus vitreus* and *Xylaria longipes*. Int Biodeterior Biodegradation 105:178–184. https://doi.org/10.1016/j.ibiod.2015.09.003
19. Esmailpour A, Taghiyari HR, Golchin M, Avramidis S (2019) On the fluid permeability of heat treated paulownia wood. Int Wood Prod J 10:55–63. https://doi.org/10.1080/20426445.2019.1617954
20. Esteves B, Marques AV, Domingos I, Pereira H (2013) Chemical changes of heat treated pine and eucalypt wood monitored by ftir. Maderas Cienc y Tecnol 15:245–258. https://doi.org/10.4067/S0718-221X2013005000020

21. Kishino M, Nakano T (2004) Artificial weathering of tropical woods. Part 2: Color change. Holzforschung 58:558–565. https://doi.org/10.1515/HF.2004.085
22. Leggate W, Kumar C, Mcgavin RL, Faircloth A (2021) The Effects of Drying Method on the Wood Permeability ,. 16:698–720
23. Leggate W, Redman A, Wood J, et al (2019) Radial permeability of the hybrid pine (*Pinus elliottii* × *Pinus caribaea*) in Australia. BioResources 14:4358–4372. https://doi.org/10.15376/biores.14.2.4358-4372
24. Lehringer C, Richter K, Schwarze FWMR, Militz H (2009) A review on promising approaches for liquid permeability improvement in softwoods. Wood Fiber Sci 41:373–385
25. Lengowski EC, Júnior EAB, Nisgoski S, et al (2020) Properties of Thermally Modified Teakwood. Maderas Cienc y Tecnol 23:1–16. https://doi.org/10.4067/S0718-221X2021000100410
26. Li Y, Xie L, Ma H (2015) Permeability and mechanical properties of plant fiber reinforced hybrid composites. Mater Des 86:313–320. https://doi.org/10.1016/j.matdes.2015.06.164
27. Mahdian M, Huang LY, Kirk DW, Jia CQ (2020) Water permeability of monolithic wood biocarbon. Microporous Mesoporous Mater 303:110258. https://doi.org/10.1016/j.micromeso.2020.110258
28. Oberhofnerová E, Pánek M (2016) Surface wetting of selected wood species by water during initial stages of weathering. Wood Res 61:545–552
29. Piao C, Winandy JE, Shupe TF (2010) From hydrophilicity to hydrophobicity: A critical review: Part I. Wettability and surface behavior. Wood Fiber Sci 42:490–510
30. Rezende RN, Lima JT, Elís L, et al (2018) Wood Permeability in *Eucalyptus grandis* and *Eucalyptus dunnii*. 25:1–7
31. Rogério M, Oliveira G De, Deiner J, et al (2010) Permeability Measuremens of Brazilian Eucalyptus. 13:281–286
32. Rossi D, Rossi S, Morin H, Bettero A (2012) Within-tree variations in the surface free energy of wood assessed by contact angle analysis. Wood Sci Technol 46:287–298. https://doi.org/10.1007/s00226-011-0407-1
33. Severiano LC, Lahr FAR, Bardi MAG, et al (2010) Influence of gamma radiation on properties of common Brazilian wood species used in artwork. Prog Nucl Energy 52:730–734. https://doi.org/10.1016/j.pnucene.2010.04.008
34. Siau (1984) Transport processes in wood. Springer, Heidelb 5:2000
35. Summerscales J, Searle TJ (2005) Low-pressure (vacuum infusion) techniques for moulding large composite structures. Proc Inst Mech Eng Part L J Mater Des Appl 219:45–58. https://doi.org/10.1243/146442005X10238
36. Taghiyari HR, Habibzade S, Miri Tari SM (2014) Effects of Wood Drying Schedules on Fluid Flow in Paulownia Wood. Dry Technol 32:89–95. https://doi.org/10.1080/07373937.2013.813855
37. Tappi (2007) Preparation of wood for chemical analysis (Revision of T 264 cm-97). T264 C 1988:3–5

38. Tappi T222 Om-02 (2011) Lignin in Wood and Pulp. In: TAPPI TEST METHODS. Technical Association of Pulp an Paper Industry. Atlanta, GA. Tappi Press. pp 1–7
39. Tappi T257 (2012) Sampling and preparing wood for chemical analysis. In: TAPPI TEST METHODS. Technical Association of Pulp an Paper Industry. Atlanta, GA. Tappi Press.
40. TAPPI T 204 cm-97 (2012) Solvent extractives of wood and pulp T 204 cm-97. TAPPI TEST METHODS Tech Assoc Pulp an Pap Ind Atlanta, GA Tappi Press 1–12
41. Tappi T 211 om-02 (2002) Ash in wood, pulp, paper and paperboard: combustion at 525°C. In: TAPPI TEST METHODS. Technical Association of Pulp an Paper Industry. Atlanta, GA. Tappi Press. pp 1–5
42. Tarmian A, Zahedi Tajrishi I, Oladi R, Efhamisisi D (2020) Treatability of wood for pressure treatment processes: a literature review. Eur J Wood Wood Prod 78:635–660. https://doi.org/10.1007/s00107-020-01541-w
43. Trindade RS, Ribeiro AC, Souza JA, Amico SC (2019) Experimental investigation of transverse permeability applied to liquid molding. Polym Compos 40:3938–3946. https://doi.org/10.1002/pc.25254
44. Valério Alvaro, Watzlawick LF, Silvestre R, Koehler HS (2008) Determinação da densidade básica da madeira de cedro (*Cedrela fissilis* Vell.) ao longo do fuste. Appl Res Agrotechnology 1:
45. Yun M, Carella T, Simacek P, Advani S (2017) Stochastic modeling of through the thickness permeability variation in a fabric and its effect on void formation during Vacuum Assisted Resin Transfer Molding. Compos Sci Technol 149:100–107. https://doi.org/10.1016/j.compscitech.2017.06.016
46. Zabel RA, Morrell JJ (2020) Chemical protection of wood (wood preservation).
47. Zanella A, Rosa M, Fioresi T, Fortes FDO (2016) Axial variation of basic density of Araucaria angustifolia wood in different diameter classes. 1969–1972
48. Zhang Y, Cai L (2008) Impact of heating speed on permeability of sub-alpine fir. Wood Sci Technol 42:241–250. https://doi.org/10.1007/s00226-007-0172-3

Figures

Figure 1

Illustration of the capillary pressure process used.

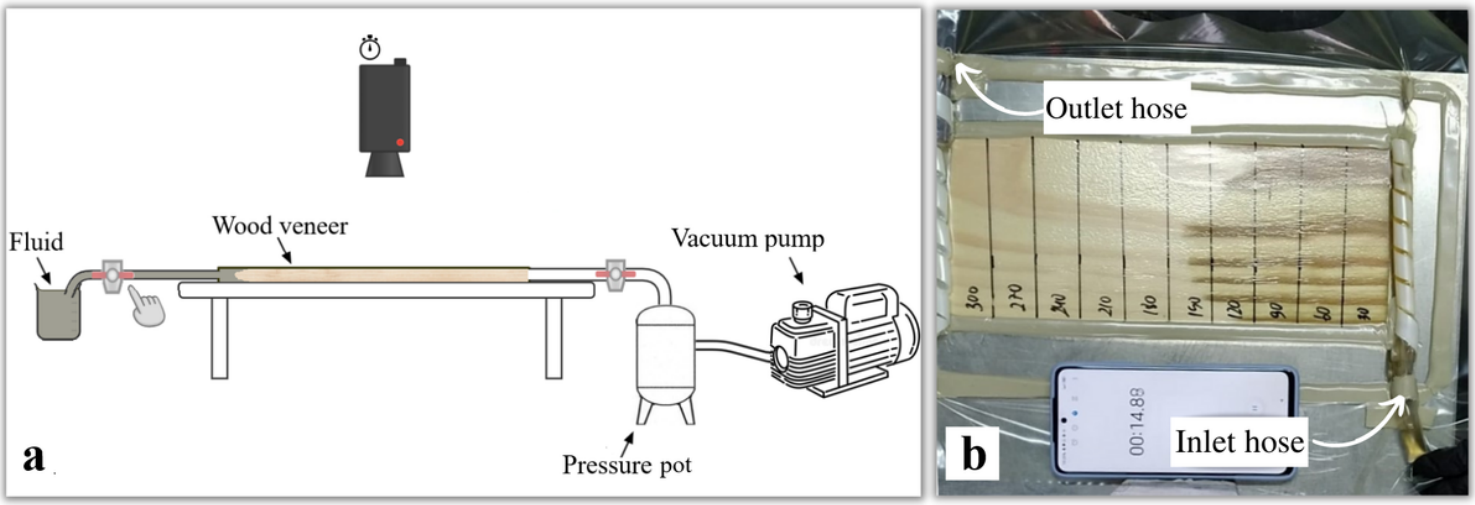

Figure 2

Illustration of the vacuum infusion process used for measuring wood permeability (a) and photo of the actual system (b).

Figure 3

Chemical properties of the woods.

Figure 4

Optical micrographs of the transverse planes of *Pinus elliottii* (a), *Araucaria angustifolia* (b), *Cedrela fissilis* (c) *Ochroma pyramidale* (d), *Tectona grandis* (e), and *Eucalyptus grandis* (f).

Figure 5

Apparent contact angle for the woods using different liquids.

Figure 6

Height of the flow front in the capillary experiments for the studied woods and fluids.

Figure 7

Squared flow front position vs. injection time data (a and b) and photos of the woods being permeated (c).

Figure 8

Squared flow front position (x_{ff}^2) vs. injection time data (a and b).

Figure 9

Apparent permeability of the studied woods (note: different letters above the bars represent significant differences).

Supplementary Files

This is a list of supplementary files associated with this preprint. Click to download.

- SupplementaryMaterial.mp4